Secondary-electron yields from thin foils: A possible probe for the electronic stopping power of heavy ions

Hermann Rothard, Kurt Kroneberger, Alexander Clouvas,* Erling Veje,† Peter Lorenzen, Norman Keller, Jürgen Kemmler, Wolfgang Meckbach,‡ and Karl-Ontjes Groeneveld
Institut für Kernphysik der Johann-Wolfgang-Goethe-Universität, August-Euler-Strasse 6, D-6000 Frankfurt am Main 90, Federal Republic of Germany
(Received 31 July 1989)

We have measured heavy-ion-induced ($Z_P = 2, 10, 18, 36, 54$; 15 keV/u $\leq E_P/M_P \leq 600$ keV/u secondary-electron (SE) yields from sputter-cleaned entrance (γ_B) and exit surfaces (γ_F) of thin solid foils (C, Al, Ti, Ni, and Cu; $d \approx 1000$ Å) in ultrahigh vacuum ($p = 10^{-7}$ Pa). A pronounced increase of the forward to backward SE yield ratio $R = \gamma_F/\gamma_B$ with increasing Z_P is observed. The SE yield to energy-loss ratio $\Lambda^* = \gamma/S_e$ has been found to be smaller for heavy ions (HI) than for light ions (H and He); i.e., $\Lambda^*(\mathrm{HI}) < \Lambda^*(\mathrm{He}) < \Lambda^*(\mathrm{H})$. Also, at low projectile velocities ($v_P^2 < 50$ keV/u), the value of Λ^* increases with decreasing v_P. The velocity and projectile dependence of both R and Λ^* can be described within simple extensions of Schou's SE emission transport theory and a semiempirical Sternglass-type model introduced by Koschar and co-workers as caused by nonequilibrium projectile energy losses S_e^* near the surfaces. The near-surface energy losses are reduced compared to tabulated bulk energy loss values S_e both for forward and backward emission under the assumption of a proportionality between SE yields and dE/dx. The Z_P-dependent reduction factors, i.e., the ratios S_e^*/S_e, as well as material parameters $\Lambda = \gamma/S_e^*$, are deduced from the SE yield measurements. Nevertheless, a rough overall proportionality $\gamma \sim dE/dx$ over four decades of both forward and backward secondary-electron yields γ and electronic energy losses dE/dx in a wide range of projectile velocities (15 keV/u $\leq E_P/M_P \leq 16$ MeV/u) and projectile nuclear charges Z_P ($1 \leq Z_P \leq 92$) is found.

I. INTRODUCTION

The bombardment of condensed matter with swift ions ($v_P/v_0 > 0.1$, v_0 Bohr velocity) leads to the interesting phenomenon of kinetic "ion-induced secondary-electron emission" (IISEE). More generally, secondary-electron creation occurs whenever ionizing radiation interacts with matter. Thus, the knowledge of secondary-electron (SE) yields as well as their energy and angular distribution is of major importance in a variety of fields. Examples are radiation physics, chemistry, and biology;[1-3] plasma-wall interactions (in particular, in relation to fusion research for controlled nuclear power production);[4,5] radiation damage and nuclear track formation;[6] ion-induced plasma-desorption mass spectrometry;[7] secondary-electron multipliers for particle detection and for precise measurements of extremely low currents; surface analysis;[8,9] and many more.

IISEE has to be taken into account whenever it is necessary to obtain the rate of charged particles by measuring their associated charge current. Thus, precise SE-yield data as well as simple relationships for a quick and easy estimate of SE yields are important for ion-beam experiments in atomic and nuclear physics and in particular for the use of ion beams for material modification and analysis.

IISEE, and especially secondary-electron emission (SEE) induced by protons, can be used to study the basic features of charged-particle interactions with condensed matter (excitation, electron transport, surface, and solid-state effects) in contrast to electron-induced SEE, because only a very small momentum transfer from the target electrons to the projectile occurs and thus no backscattering of projectiles by the target electrons has to be considered. This means that IISEE can serve as a good test for SEE theories, which can also be applied to such fields as scanning electron microscopy and all kinds of surface analysis with Auger, photo, or secondary electrons. Actually, some protons will be backscattered from the heavy atoms of, e.g., a gold target. These protons pass twice through the entrance surface, creating SE's each time. However, the contribution of these Rutherford-backscattered projectiles to the total SE yield will be small compared to the total yield, and can be neglected.

In this context, experiments on SEE from thin foils yield more fundamental information (compare also Sec. IV C) than the study of SEE from thick samples in the backward direction only, because a considerable proportion of the projectile energy loss leads to the creation of high-energy δ electrons, which are predominantly ejected in the forward direction. Furthermore, some features of IISEE can be observed only in the forward direction, e.g., "convoy electrons"[10] or "shock electrons," the latter ones originating from the ion-induced collective excitation of the target-electron plasma ("wake").[11-14] Also, nonequilibrium conditions of the charge and excitation states of the ion can be probed with SE if the target thickness is in the order of or smaller than the (average) mean free path of the studied electrons.

The SE yield γ is defined as the average number of SE

emitted per incoming projectile. The yield of SE's in the backward direction emitted in the backward hemisphere γ_B, from thick samples (i.e., thicker than the range of the ions or associated electrons) bombarded with protons and heavy ions has been studied as a function of the projectile velocity v_P, the projectile nuclear charge Z_P, the charge state of the ion q_i, the angle of incidence of the beam δ, and the target material Z_T.[15,16]

It was found that γ depends on both surface composition and topology.[8,15,16] Thus, experiments with controlled surfaces under ultrahigh vacuum are necessary.

SEE was described as early as in 1899,[17] and was recognized around 1905.[18–20] Although IISEE from thin foils was first investigated in 1931,[21] only a few papers have been published concerning measurements of the total secondary-electron yield $\gamma_T=\gamma_B+\gamma_F$ with thin-foil targets.[22–27] Here, γ_F is the yield of SE emitted in the forward hemisphere, i.e., the yield from the surface where the ions exit from the foil. In these experiments, γ_T has been studied as a function of v_P, Z_T, δ, and the target thickness d with different projectiles. Also, it has been found that the target temperature affects γ_T.[28–30]

Some authors have studied separately the emission of SE from both the entrance and the exit surfaces of thin foils[31–42] and deduced the ratio of forward to backward SE yields $R=\gamma_F/\gamma_B$. The ratio R, introduced by Meckbach, Braunstein, and Arista in 1975,[34] has been studied as a function of v_P with different ions and target materials, but the data are scattered over a broad range of ion-atomic numbers, velocities, target materials, and ion charge states.[31–42] Thus, no clear picture arises concerning the v_P, Z_T, and Z_P dependences of γ_F and γ_B and their relationship. Only two groups have yet been able to perform experiments with thin foils in ultrahigh vacuum with controlled surface conditions.[24,34,40,41]

Common to nearly all theoretical approaches[1,32,43–47] is the division of the processes leading to SEE in the following steps.

(i) Production of "internal SE" in the bulk of the solid by (a) primary ionization caused by collisions of the bombarding projectiles with target electrons (target ionization) (also, projectile ionization can occur if the projectile carries electrons); and (b) secondary ionization by internal SE (and in particular high-energy δ electrons), recoil ions, and possibly photons. This step is related to the electronic energy loss per unit path length $-dE/dx:=S_e$ (expressed in units of eV/Å) of the ions in condensed matter and, if there is a non-negligible contribution of SE induced by recoil ions, also to the nuclear stopping power S_n.

(ii) Transport of the SE through the bulk of the target to the surface.

(iii) The transmission of SE through the surface potential barrier.

Furthermore, one has to consider that the ions undergo charge-exchange processes until a dynamic charge equilibrium inside the solid foil is reached. The measurement of SE yields from foils as a function of the target thickness d provides a powerful tool to study this preparation[48] of the ion beam, i.e., the evolution of ion charge states together with charge exchange processes related to nonequilibrium stopping powers.[31,32,48]

It is important to note that similar nonequilibrium processes also take place at the exit surface. The effective charge of the ions inside the solid generally differs from their mean charge outside the solid, and thus charge-exchange processes also happen "near the surface," i.e., in the last atomic layers of the foil.

Furthermore, the surface cannot be considered as a simple step where suddenly the bulk of the solid ends and the vacuum begins. Rather, there is a slow transition between the bulk and the vacuum. In this near surface region, the density and also the electronic properties of the target (as well as the screening of the projectile charge) and thus the charge state of the ions can change.

As a main feature, the most frequently applied theoretical models[43–45] consider γ to be proportional to the electronic stopping power S_e, i.e.,

$$\gamma/S_e=\text{const} . \tag{1}$$

It is common practice to define parameters Λ^* as ratios between the measured SE yields and the (tabulated) stopping-power values to study the validity of Eq. (1) as a function of v_P, Z_P, and Z_T,

$$\begin{aligned}\Lambda_T^*&=\gamma_T/S_e ,\\ \Lambda_B^*&=\gamma_B/S_e ,\\ \Lambda_F^*&=\gamma_F/S_e ,\end{aligned} \tag{2}$$

for the total, backward, and forward SE yields, respectively. For electron[15] and low-velocity ($v_P<v_0$) heavy-ion[49] impact, Λ_B^* has been shown to depend on the projectile velocity; for proton bombardment, however, Eq. (1) has been confirmed experimentally within about 10% both for γ_B (Refs. 15, 16, and 50 and γ_T (Ref. 24) in the wide projectile energy range of 10 keV/u $\le E_P/M_P \le$ 24 MeV/u (projectile energy E_P, projectile mass M_P). In this case, i.e., for protons the parameters Λ_T^* and Λ_B^* could then be expected to depend only on target properties such as ionization cross sections, transport lengths for secondary particles in condensed matter, and the surface-dependent escape probabilities. This would mean that $\Lambda_{T,B}^*$ may be considered as "material parameters" for the particular case of proton impact.

With heavy ions, deviations from the simple rule given by Eq. (1) have been observed, especially at low projectile velocities, i.e., $v_P^2/2=E_P/M_P<150$ keV/u.[15,23,49] Λ_B^* was found to depend on the projectile atomic number Z_P,[15,49] and, in accordance with the establishment of charge equilibrium and the consequent adjustment of stopping powers close to the entrance surface of the solid target, on the charge state of the incoming projectiles, or the "partial stopping powers" that are characteristic for these charge states.[32]

In the following, we present experimental studies of secondary-electron yields γ_B (in the backward direction) and γ_F (in the forward direction) from thin solid foils ($d\approx 1000$ Å) bombarded with heavy ions of incident charge state $q_i=+1$. The foils were thick enough to ensure charge equilibration of the ions at the exit surface and thicker than ranges of the low-energy SE produced

inside the solid, but much thinner than the mean ranges of the ions. The SE coefficients γ_F and γ_B have been measured as functions of the projectile nuclear charge ($Z_P=2,10,18,36,54$), the target material (C, Al, Ti, Ni, and Cu), and the projectile velocity (15 keV/u $\leq E_P/M_P \leq$ 600 keV/u) from sputter-cleaned target surfaces under ultrahigh vacuum conditions ($p=10^{-7}$ Pa) because of the following reasons.

(i) The first motivation was to obtain absolute values of heavy-ion-induced SE yields in the velocity regime of 15 up to 120 keV/u.

(ii) The second motivation was to test whether the important basic relation Eq. (1) predicted by theory and confirmed by experiment for proton impact also holds for heavy ions: Is the heavy-ion-induced SE yield proportional to the electronic energy loss S_e as a function of the projectile velocity v_P, i.e., is $\Lambda^*(v_P)=$const? And, is there a Z_P dependence of Λ^*, i.e., is Λ^* really a "material parameter"?

(iii) However, the most important motivation for this work was to study systematically the projectile (Z_P) and also the target material (Z_T) dependence of the ratio $R=\gamma_F/\gamma_B$. Can the results be understood in the framework of the frequently cited and applied theoretical models of Sternglass,[43] Schou,[44,45] and the extended Sternglass-type model of Koschar *et al*?[32]

II. EXPERIMENT

The experimental setup is similar to the one presented in Ref. 31, except that, here, the experiments have been performed in an ultrahigh-vacuum chamber ($p=10^{-7}$ Pa) at the 2.5-MV Van de Graaff accelerator of the Institut für Kernphysik der Johann-Wolfgang-Goethe-Universität in Frankfurt am Main. The accelerator facility delivered singly charged He^+, Ne^+, Ar^+, and Xe^+ ions in the specific energy ranges 90–600, 15–120, 15–60, 15–30, and 15 keV/u, respectively. More details are described elsewhere.[42]

Two nearly closed metal cylinders (similar to Faraday cages, except for openings for the incoming and outgoing ion beam) mounted on each side of a target-foil holder were used to collect the SE's in forward and backward directions of the target foil simultaneously. The cylinders were held at a positive potential of +40 V to assure that all the SE's were collected, and a negative potential of −40 V was applied to the target to avoid influences due to contact or surface potentials (compare Ref. 31). The

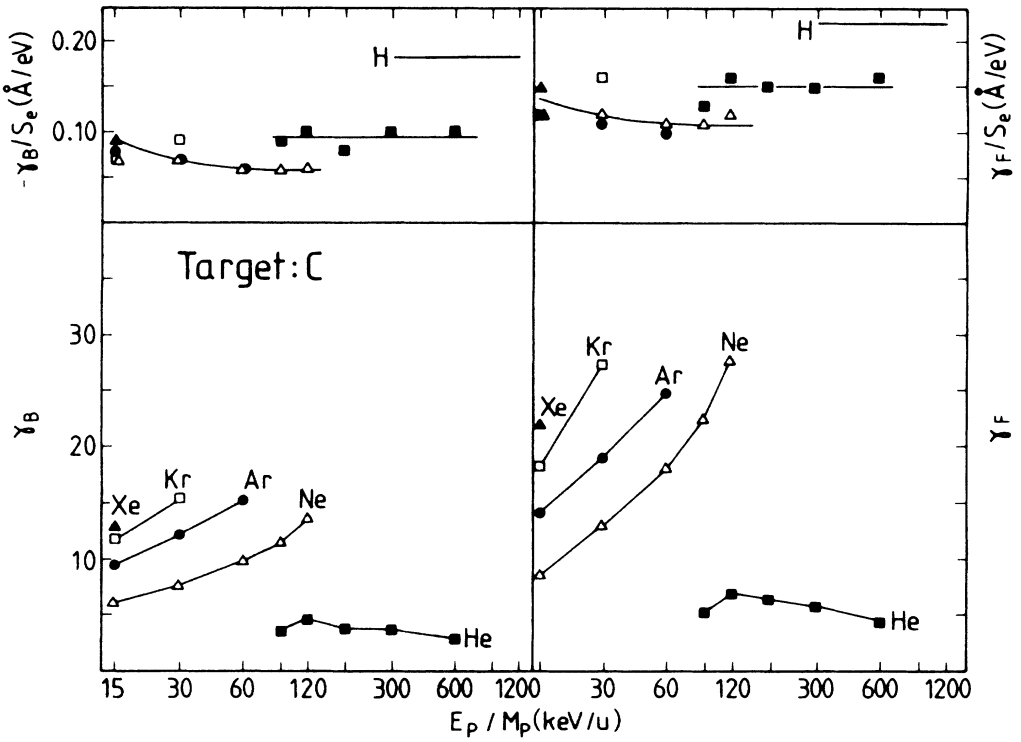

FIG. 1. Heavy-ion-induced (Xe, Kr, Ar, Ne, and He) secondary-electron yields (lower part) from the sputter-cleaned entrance (γ_B, left) and exit surfaces (γ_F, right) of thin C foils ($d \approx 1000$ Å) as a function of the square of the projectile velocity $\frac{1}{2}v_P^2=E_P/M_P$. The upper parts show the corresponding secondary-electron yield to projectile energy loss ratios $\Lambda^*=\gamma/S_e$ (solid triangles, Xe; open squares, Kr; solid circles, Ar; open triangles, Ne; solid squares, He). The solid lines are to guide the eye and represent mean values in the case of Λ^*(He). Also, mean Λ^* values for H projectiles (300–1200 keV/u) taken from Ref. 40, which were obtained with the same experimental setup, have been included in the figure.

SE currents collected in the cylinders were normalized to the current measured at an antiscattering aperture (i.e., an aperture that also serves to intercept scattered incoming beam particles) upstream of the target. A normalization to the number of projectiles was achieved from the ratio of the aperture current to the ion-beam current measured with a Faraday cup without target.[42,51] The sum of the SE yields γ_B and γ_F measured with the cylinders in the forward and backward directions was equal within 8% to the total SE yield γ_T obtained by measuring the target current and correcting for the charge changing of the ions.[22,31] The error is estimated to be $\pm 12\%$ for all the SE yields and the error for the R values is $\pm 25\%$.

The thin, self-supporting target foils of C, Al, Ti, Ni, and Cu were produced by standard evaporation techniques. The bombardment of the targets with heavy noble-gas ions results in a cleaning of both target-foil surfaces by backward and forward (transmission) sputtering. The removal of the contamination of the target surfaces with C and O (most probably as hydrocarbons and water) could be controlled by the following two independent methods.

(i) Rutherford-forward-scattered ions (H,He) could be detected with a UHV-compatible bakeable silicon detector mounted at an observation angle of 35° with respect to the beam, which could "see" the target through a small hole in the forward cylinder. This detector was also used to check the target thickness.

(ii) The secondary-electron yields themselves can be used as a measure for the surface contamination: When bombarding a fresh surface, the SE yields decrease until they reach a minimum saturation value indicative for a cleaned surface.[8,9,51]

All the results reported here have been obtained from sputter-cleaned surfaces with minimum secondary-electron yields and when no more surface contamination could be detected by Rutherford scattering. We estimate the residual surface contamination to be lower than 0.1 monolayer of C or O.

III. RESULTS

A. Secondary-electron yields

The lower parts of Figs. 1–5 show the SE yields γ_B (left) and γ_F (right) for the five target materials (C, Al, Ti, Ni, and Cu) as a function of the specific energy (i.e., the projectile energy per unit mass) E_P/M_P [i.e., the square of the projectile velocity $v_P^2/2$). We observe the following.

(i) In agreement with the findings of Ref. 40 for hydrogenic projectiles, for a given projectile velocity γ_F is always higher than γ_B for all projectile-target combinations; i.e., the SE emission in the forward direction dominates.

(ii) Both γ_F and γ_B increase with v_P for Ne (15 keV/u $\leq v_P^2/2 \leq$ 120 keV/u), Ar (15 keV/u $\leq v_P^2/2 \leq$ 60 keV/u), and Kr (15 keV/u $\leq v_P^2/2 \leq$ 30 keV/u) in the energy ranges accessible for measurement. For Xe, only one measurement at 15 keV/u could be performed. For He our measurements, which cover the range 90

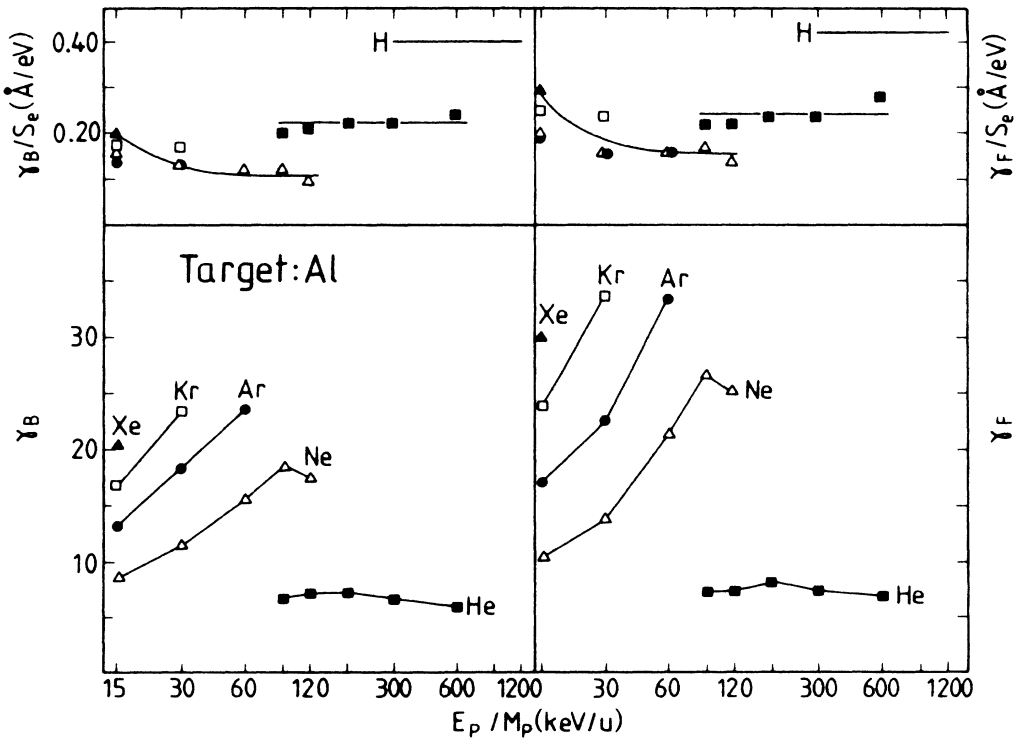

FIG. 2. Same as Fig. 1, for an Al foil.

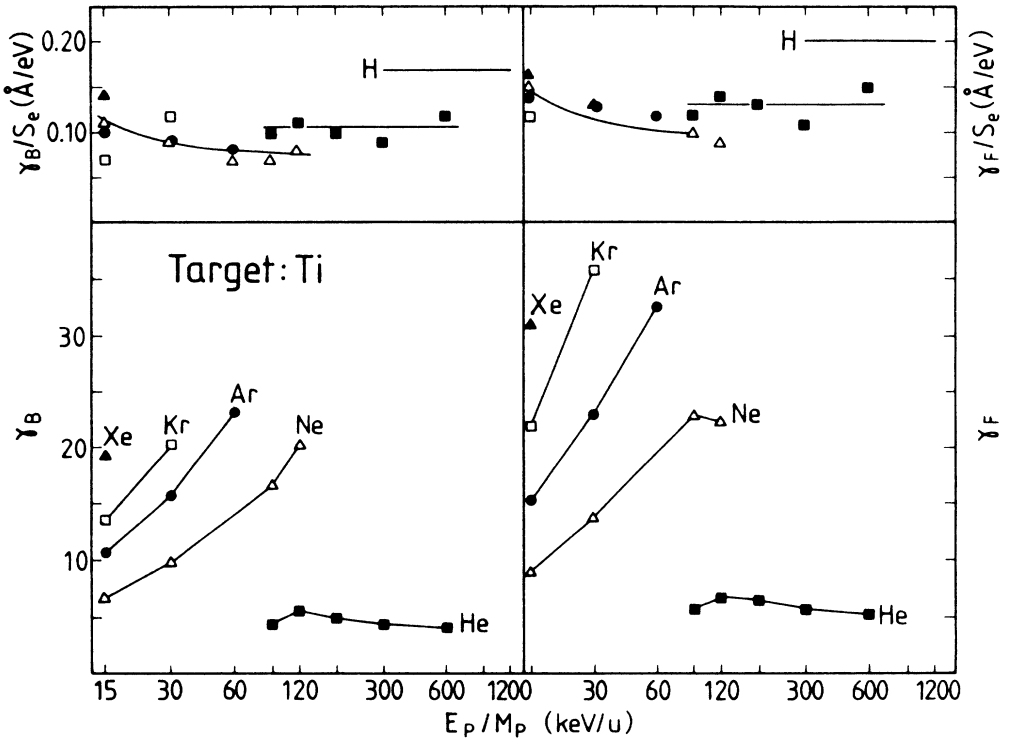

FIG. 3. Same as Fig. 1, for a Ti foil.

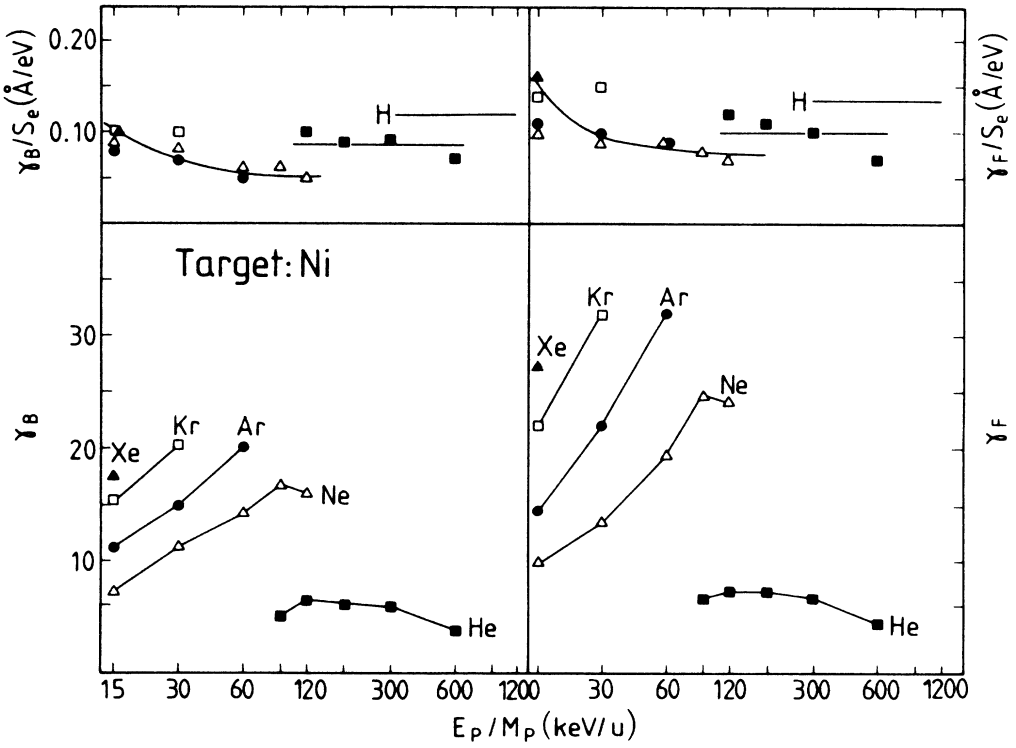

FIG. 4. Same as Fig. 1, for a Ni foil.

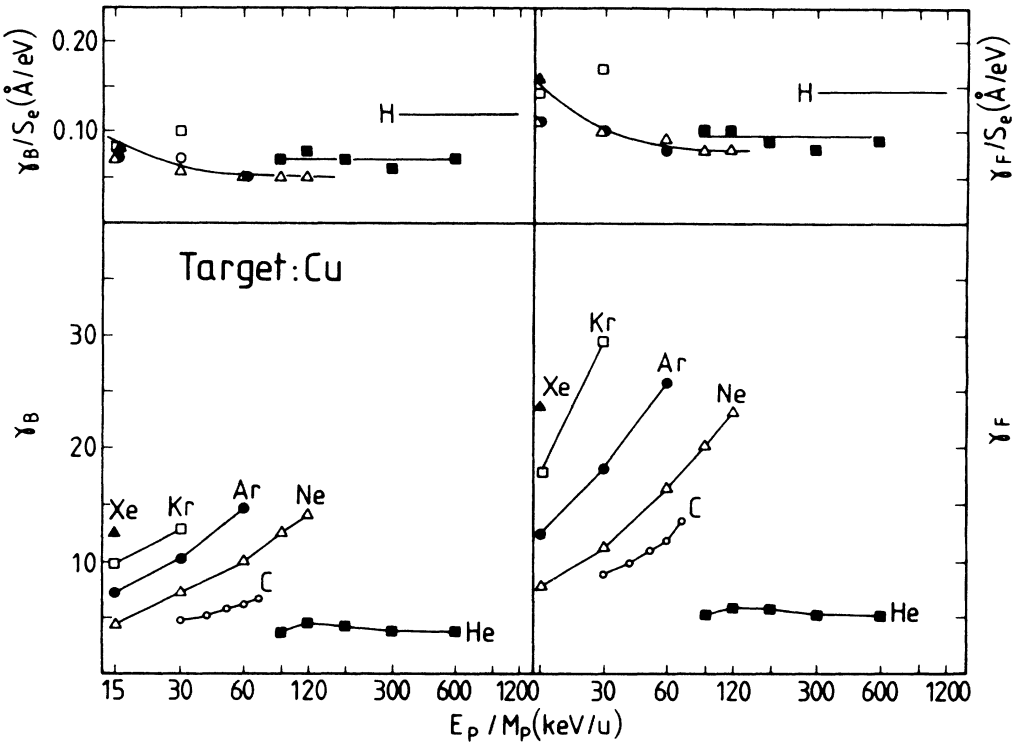

FIG. 5. Same as Fig. 1, for a Cu foil. The C^+ data have been included for comparison and are taken from Ref. 40.

keV/u $\leq v_P^2/2 \leq 600$ keV/u, show an increase of γ_F and γ_B with v_P to a maximum yield in the vicinity of $E_P/M_P = v_P^2/2 \approx 120$ keV/u followed by a slight decrease. According to Ref. 52 this maximum would correspond to the known maximum of S_e in this energy range.

(iii) γ_F and γ_B show a weak dependence on Z_T, but this is not a simple function of Z_T as, e.g., an increase or decrease with Z_T. A general trend is $\gamma(\text{Al}) > \gamma(\text{Ni}) \approx \gamma(\text{Ti}) > \gamma(\text{C}) \approx \gamma(\text{Cu})$, but this does not hold for all v_P and Z_P.

(iv) There is a remarkable dependence of γ_F and γ_B on the projectile atomic number at a given velocity and for a given target material; both SE yields increase strongly with Z_P. For the heavier ions Ne, Ar, Kr, and Xe and in the case of forward emission, γ_F can be up to ten times larger than the yield obtained with He and, as can be deduced from Refs. 24 and 40, with H.

B. Secondary-electron yield to energy-loss ratio

The upper parts of Figs. 1–5 show the $E_P/M_P = v_P^2/2$ dependence of the parameters $\Lambda_{F,B}^* = \gamma_{F,B}/S_e$. The stopping-power values have been calculated according to Ref. 52. Also, the mean Λ^* value for protons obtained with the same experimental setup from Ref. 40 are included. The following can be seen.

(i) $\Lambda_{F,B}^*(v_P)$ are constant above $E_P/M_P = v_P^2/2 > 50$ keV/u, i.e., the velocity dependence of γ follows that of the energy loss S_e, except at low velocities.

(ii) At low velocities, i.e., $E_P/M_P = v_P^2/2 < 50$ keV/u, there is, for Ne, Ar, Kr, and Xe, a decrease of $\Lambda_{F,B}^*$ with increasing velocity. (This velocity range is not covered by the measurements with He.) Due to their energy loss, the heavy ions have a lower velocity at the exit surface and thus a reduced γ_F compared to ions with a somewhat higher velocity (equal to the velocity at the entrance surface), because we are in the velocity region below the stopping-power maximum. Thus, when correcting for the energy loss of the heavy ions in the foils, the increase of the Λ^* parameters becomes even more pronounced.

(iii) $\Lambda_{F,B}^*$ depend on the projectile nuclear charge Z_P. The "saturation values" of $\Lambda_{F,B}$ are systematically lower for the heavier ions compared with He and H. In Table I, we compare the parameters Λ_F^* and Λ_B^* as well as $\Lambda_T^* = \Lambda_F^* + \Lambda_B^*$ for protons (H) (data again taken from Ref. 40), helium ions (He), and heavy ions (HI). Here and in the following, the mean Λ^* values for Ne and Ar will be discussed, since we found $\Lambda_{F,B}^*(\text{Ne}) \approx \Lambda_{F,B}^*(\text{Ar})$ within the experimental error bars. This has been observed previously, too.[24,49] Also, the $\Lambda_{F,B}^*$ values of Kr and Xe were found to fall close together, but they are smaller than those of Ar and Ne.[49] For Kr and Xe saturation was not reached within the present measurements.

In Table I some Λ^* values obtained by other authors have been included (in parentheses) for comparison; see also Secs. IV B and IV D. In the case of C, Ni, and Cu, the agreement is fairly well within 20%, but in the cases of Al and Ni, deviations of up to 60% appear. We note from Table I as a main result that $\Lambda^*(\text{HI}) < \Lambda^*(\text{He}) < \Lambda^*(\text{H})$ for γ_F, γ_B, γ_T, and all target materials.

TABLE I. Mean backward, forward, and total secondary-electron yield to projectile energy-loss ratios $\Lambda_B^*=\gamma_B/S_e$ (Å/eV), $\Lambda_F^*=\gamma_F/S_e$ (Å/eV), and $\Lambda_T^*=\gamma_T/S_e$ (Å/eV) for different targets (C, Al, Ti, Ni, and Cu). The data in parentheses have been included for comparison.

Target	Protons	Helium	Heavy ions
	$\Lambda_B^*=\gamma_B/S_e$ (Å/eV)		
C	0.18 (0.122)[a]	0.095	0.060
Al	0.40 (0.118)[a]	0.23 (0.084)[b]	0.11 (0.068)[b]
Ti	0.17 (0.068)[a]	0.11	0.075
Ni	0.12	0.080	0.050
Cu	0.12 (0.091)[a]	0.085 (0.053)[c]	0.050 (0.041)[c]
	$\Lambda_F^*=\gamma_F/S_e$ (Å/eV)		
C	0.22	0.15	0.11
Al	0.43	0.24	0.16
Ti	0.20	0.13	0.10
Ni	0.13	0.095	0.080
Cu	0.14	0.10	0.075
	$\Lambda_T^*=\gamma_T/S_e$ (Å/eV)		
C	0.40 (0.53)[d]	0.25	0.17
Al	0.83 (0.48)[d]	0.47	0.27
Ti	0.37	0.24	0.18
Ni	0.25 (0.30)[d]	0.18	0.13
Cu	0.26 (0.23)[d]	0.16	0.14

[a]Reference 15.
[b]Reference 64.
[c]Reference 49.
[d]Reference 24.

C. Forward to backward secondary-electron yield ratio

In Figs. 6–10 the ratio $R=\gamma_F/\gamma_F$ is plotted in the studied velocity range 15 keV/u $\leq v_P^2/2 \leq$ 120 keV/u as a function of $E_P/M_P=v_P^2/2$. Again, proton data obtained with the same experimental setup from Ref. 40 have been included.

(a) For the heavier ions Ne, Ar, and Kr, a general trend is that R either increases with v_P (C, Fig. 6; Ni, Fig. 9) or that it remains constant over the whole studied v_P range (Al, Fig. 7; Ti, Fig. 8; Cu, Fig. 10) within the error limits of 25%. In the case of He ions, R remains constant. It has been observed previously[34,36,38] that R reached a saturation value at some hundred keV/u, and our data are consistent with a saturation value of R around $E_P/M_P \approx 100$–200 KeV/u. However, we note that the findings obtained with different targets are not the same.

(b) First of all, we compare the ratios R obtained with different projectiles traversing a Cu foil (Fig. 10). It is seen that the velocity dependence of R is, within error limits, essentially independent of the studied projectiles. This allows us to draw the important conclusion that the ratio $R=\gamma_F/\gamma_B$ increases with increasing projectile nuclear charge Z_P by up to a factor of 2 in the range $1 \leq Z_P \leq 54$. This is an important new result of this study.

The increase of the forward to backward ratio for heavier ions can be considered as further enhanced compared to values obtained with protons when considering (i) that the R values for the heavier ions Ne, Ar, Kr, and Xe are obtained in a velocity region where a possible saturation of $R(v_P)$ may not yet have been reached, and (ii) that due to the energy loss of the heavy ions they have a lower velocity at the exit surface and thus a reduced γ_F compared to ions with a somewhat higher velocity (compare with case (ii) of Sec. III B).

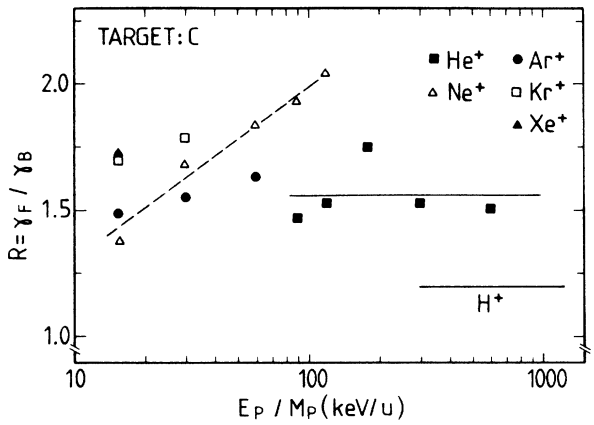

FIG. 6. Forward to backward secondary-electron yield ratio $R=\gamma_F/\gamma_B$ for different heavy ions (as indicated in the figure) as a function of the square of the projectile velocity $(\frac{1}{2})v_P^2=E_P/M_P$; target, C. The solid lines represent mean values, the dashed lines are to guide the eye. Also, the mean R value for H^+ (300–1200 keV/u) taken from Ref. 40, which was obtained with the same experimental setup, is shown in the figure.

For the case of Ni we observe in Fig. 9 that there is also a remarkable enhancement of R with increasing Z_P. However, whereas for H and He projectiles R is independent of v_P for H and He, for the heavy ions on Ni there is a systematic increase with increasing projectile velocity v_P. In this connection we may call attention to the different valence-electron configuration of Ni compared to Cu.

For the targets C, Al, and Ti (Figs. 6–8) one can con-

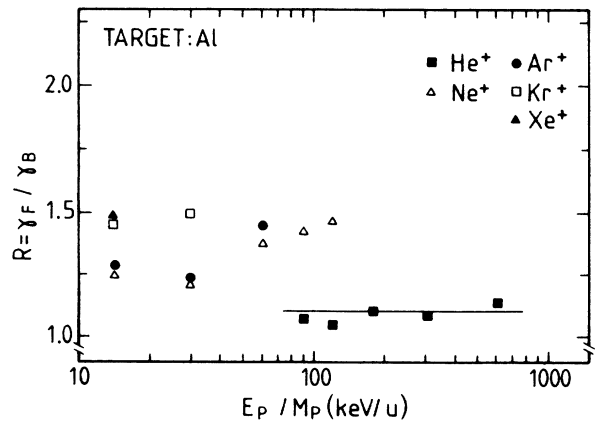

FIG. 7. Same as Fig. 6; target, Al. Since the value of $R(H^+)$ falls close to the value of $R(He^+)$, it is not shown in the figure (see Fig. 11).

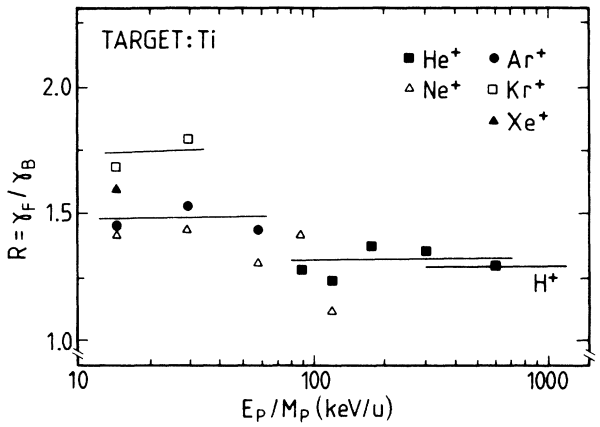

FIG. 8. Same as Fig. 6; target, Ti.

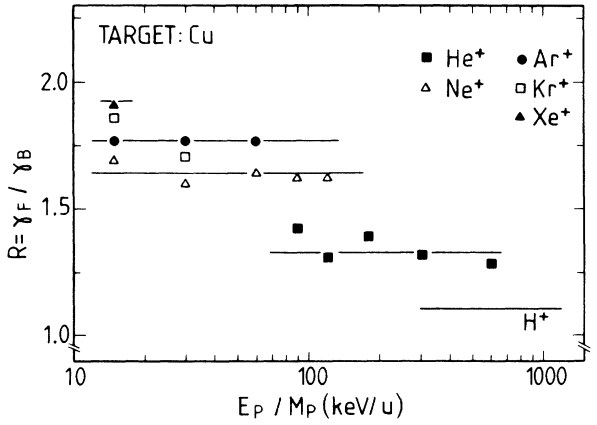

FIG. 10. Same as Fig. 6; target, Cu.

clude that there is also an overall enhancement of R with increasing projectile atomic number. A typical dependence on v_P can, however, not be seen, except for the independence of R on v_P for the case of He projectiles, which actually is verified for all targets used.

In Fig. 11, we show mean values of R from Figs. 6–10 plotted as a function of Z_P ($Z_P = 1, 2, 10, 18, 36, 54$) which give clear evidence of the mentioned increase of the forward-backward SE emission ratio.

(c) Note that there is only a weak Z_T dependence of R.

IV. DISCUSSION

A. Velocity dependence

First of all, it is significant that the values of $\Lambda^* = \gamma / S_e$ (upper parts of Figs. 1–5) agree within experimental errors at high projectile velocities, say, $E_p / M_p = v_P^2 / 2 > 50$ keV/u, in spite of the large differences in SE yields γ_F and γ_B found in the lower part of Figs. 1–5 for different heavy projectiles. This means that the SE yields γ_F and γ_B scale as the stopping powers of the respective projectiles. However, the Λ^* found for He are systematically larger than those of Ne in the region of overlap.

With respect to the dependence on v_P, both forward and backward SE yields follow the velocity dependence of the projectile energy loss even in the present case of heavy-ion impact, as can be seen from the velocity-independent constant values of $\Lambda^* = \gamma / S_e$ in the top of Figs. 1–5. It is then evident from the present measurements that the linearity between stopping power and both forward and backward SE yields [Eq. (1)] holds, not only for protons, but also for different heavy ions (with high projectile velocities $E_P / M_P = v_P^2 / 2 > 50$ keV/u) traversing different target materials. Thus, the theoretical models[32,43–45] can also be applied to heavy-ion-induced SEE, at least concerning the velocity dependence.

At lower velocities, γ is higher than expected from Eq. (1) if tabulated electronic stopping powers[52] are used. One important reason for the enhancement may be the *contribution of recoil-ion cascade-induced* SE to the total SE yield.[23] This phenomenon is related to the nuclear stopping and thus should become more important with

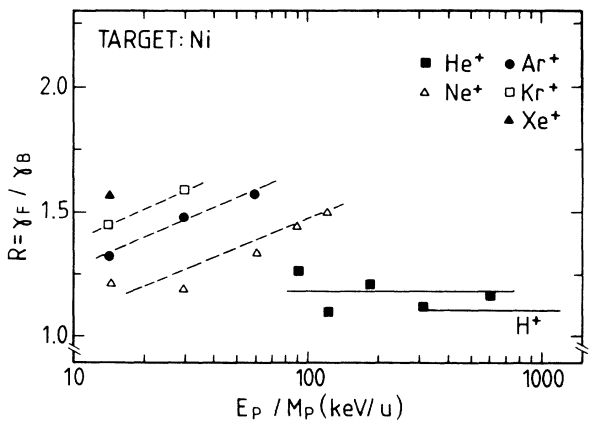

FIG. 9. Same as Fig. 6; target, Ni.

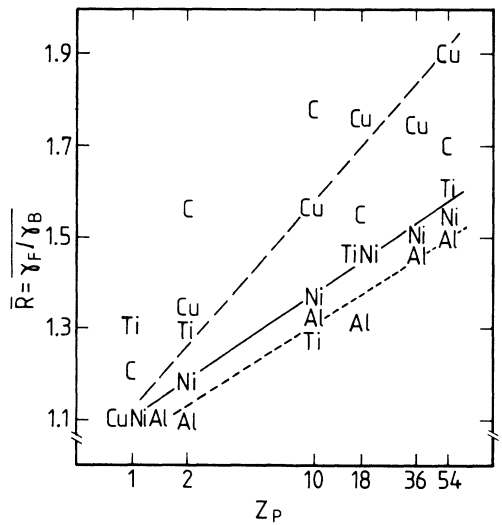

FIG. 11. The mean values of the forward to backward secondary-electron yield ratio $R = \gamma_F / \gamma_B$ as a function of the nuclear charge Z_P for different target materials (C, Al, Ti, Ni, and Cu) as indicated in the figure. The proton data are taken from Ref. 40. The lines are to guide the eye.

decreasing v_P. The contribution of recoils has been investigated in detail experimentally and has been described with a semiempirical model by Holmén *et al.*[49]

Other possible explanations have been mentioned by Frischkorn and Groeneveld,[23] e.g., a transition from the cascade electron regime to single ionization processes (see also the discussion for the v_P dependence of R below), or enhanced molecular-orbital ionization in heavy symmetric collision systems. This would alter the internal SE energy distribution, in contrast to the assumptions of the theoretical models,[44,45] where the shape of the SE energy distribution comes out to be independent of the projectile velocity or charge, which both only determine the absolute value as scaling factors. Further conclusions can only be drawn from measurements of the energy and angular distributions of heavy-ion-induced SE both at low and high projectile velocities (keV/u to some 10 MeV/u range).[28]

It is worth noting that the maximum SE yield for protons is reached at a velocity around $E_P/M_P=v_P^2/2 \approx 80-120$ keV/u close to the stopping-power maximum depending on the target material.[15] In the present experiment, a maximum SE yield for He impact is reached at $E_P/M_P=v_P^2/2\approx 120$ keV/u, but the energy-loss maximum of the heavier ions Ar, Kr, and Xe is not yet reached. However, a tendency of γ to decrease can be seen for some targets with Ne ions at velocities of $E_P/M_P=v_P^2/2>120$ keV/u (Figs. 2–4).

With reference to the forward-backward emission ratio $R=\gamma_F/\gamma_B$, according to the extended semiempirical SEE model of Koschar *et al.*[32] and following Sternglass[43], this ratio can be expressed as

$$R=\frac{\gamma_F}{\gamma_B}=\frac{S_{eF}^*}{S_{eB}^*}\frac{1}{1-\dfrac{B}{1+(\lambda_{SE}/\lambda_\delta)}} \tag{3}$$

with

$$S_{eF}^*\sim(q_{\text{eff},F})^2\ ,\qquad S_{eB}^*\sim(q_{\text{eff},B})^2\ . \tag{4}$$

The quantities S_e^* are nonequilibrium projectile energy losses[32] (compare with Sec. IV C) and are proportional to the square of the effective charges of the ions near the surface $(q_{\text{eff}})^2$. The factor B describes the partition of the projectile energy loss in two different types of collision processes, (i) close collisions between the projectile and the electrons leading to—mostly forward-directed–high-energy δ electrons (fraction BS_e), and (ii) distant collisions corresponding also to long-range collective excitations leading to—mostly isotropic—low-energy SE [fraction $(1-B)S_e$].

Thus B is connected to step (a) mentioned in the Introduction (Sec. I), i.e., the production of internal SE by primary ionization. B should not be confused with the factor β (which is connected to energy transport by fast electrons) appearing in Schou's theory.[44,45] It is worth noting that also the velocity dependence of β could account for the increased Λ^* at low velocities (compare Sec. IV C). Following Bohr,[53] an equipartition $B=(1-B)=0.5$ was chosen in the original Sternglass ansatz. The attenuation lengths λ_{SE} and λ_δ are characteristic for the high-energy δ electrons or the low-energy SE, respectively. Typical values are $\lambda_{SE}\approx 15$ Å and $\lambda_\delta\approx 300$ Å for a specific projectile energy of 1 MeV/u.[32]

Equation (3) furnishes at least a possibility for a qualitative understanding of the velocity dependence of R.[39] The ratio $\lambda_\delta/\lambda_{SE}$ can be estimated from[39,43]

$$\lambda_\delta/\lambda_{SE}\approx 5.4E_P/M_P\ , \tag{5}$$

with E_P/M_P measured in units of MeV/u.

According to Eqs. (3) and (5), R increases with increasing v_P and reaches a saturation value at high velocities with $\lambda_\delta \gg \lambda_{SE}$. From Eq. (5) it follows that $\lambda_\delta > \lambda_{SE}$ and thus a saturation of $R(v_P)$ can be expected for velocities $\frac{1}{2}v_P^2=E_P/M_P>200$ keV/u. The present data (Figs. 6–10) indicate a saturation of $R(v_P)$ at projectile velocities around $\frac{1}{2}v_P^2=E_P/M_P\approx 100-200$ keV/u. This seems to be a reasonable agreement considering that the Sternglass theory is strictly valid at high projectile velocities $v_P>2Z_Pv_B$. The weak Z_T dependence of R may have an explanation in a Z_T dependence of the electron transport lengths λ_{SE} and λ_δ.

Also, the effective energy loss S_e^* and, in particular, the partition factor B may depend on v_P. However, at low velocities $v_P<v_F$ (v_F is the velocity of the nearly free electrons around the Fermi energy level), the projectile cannot directly cause collective excitations such as plasmons or electron density fluctuations (wake[11–14]). Thus B will increase with decreasing v_P. This leads to an increased R value, in contrast to our observations. Furthermore, the dynamic screening of the projectile by the target electrons may influence the ratio R. Also, a lost projectile electron may contribute to the SE yield from the entrance surface with around 0.6 additional SE.[31] From the reasonable validity of Eq. (3) we can draw the important conclusion that SE transport in solids is of major importance for the quantitative description of the projectile velocity dependence of SE yields.

B. Target material dependence

The dependence of both γ_B and γ_T on the target atomic number Z_T (for a given projectile velocity) has been studied with protons, molecular ions, and heavy ions.[15,24,54] Oscillatory behavior of $\gamma(Z_T)$ has been observed, and also in the present experiment, no "simple" monotonic dependence [i.e., such that $Z_T(1)>Z_T(2)\Rightarrow\gamma(1)>\gamma(2)$] can be seen. This finding may be caused by a Z_T dependence of all the quantities having an influence on SEE, as, e.g., dE/dx related to the cross sections for ionization processes, electron-transport mean free paths λ, and the surface potential barrier. Furthermore, *shell* and *band structure* effects[16,54] as well as *collective* excitations like plasmon decay[55] and wake effects[11–14] may have to be considered.[16] In particular, the different valence-electron configuration of the different target materials may play an important role for both energy loss and SEE. We follow Hasselkamp[16] when concluding that "this problem is unsolved at

present and should be investigated further." This also holds for the Z_T dependence of R.

However, for different target materials ($Z_T=6$, 22,28,29) we find similar Λ_T^* values with a mean value of $\Lambda_T^*=0.32$ Å/eV. The Λ_T^* value for the Al target is higher than can be expected from values obtained with thick samples of elemental Al.[16] The most plausible reason for this finding is that Al may be contaminated by oxygen in the bulk of the target originating from the target production by evaporation.

With respect to a dependence of the forward-backward emission ratio on the target (Z_T) no clear conclusion can be drawn because of the differences found in the dependencies of R on V_P. An exception is the case of He projectiles, for which R is independent of v_P (Figs. 6–10). However, in this case, $R(Z_T)$ approximately follows the Z_T dependence of the first ionization energy. More measurements are needed to confirm such a similarity, which may be related to the fact that more violent collisions are favored in the production of forward emitted SE.

C. Projectile dependence

In the following, we will show that the important results (iii) of Sec. III B and (b) of Sec. III C, i.e., the Z_P dependence of Λ^* and R, can be described within the framework of Schou's theory for SEE.[44,45] According to this transport theory, the (fast) proton-induced SE yields are given by

$$\begin{aligned}\gamma_F&=\Lambda\beta_F S_e\ ,\\ \gamma_B&=\Lambda\beta_B S_e\ ,\\ \gamma_T&=\Lambda S_e\ ,\end{aligned}\tag{6}$$

in analogy with Eqs. (1) and (2).

The difference in the forward and backward emission is contained in the dimensionless factors β_F and $\beta:=\beta_B$ in such a way that $D_{F,B}=\beta_{F,B}S_e$ is the energy deposited in the kinetic energy of electrons due to the energy loss S_e of the projectiles near the exit (downstream) and the entrance (upstream) surfaces, respectively. According to calculations shown in Ref. 44, β can be expected to be approximately the same for different ion-target combinations (within 15%) at specific ion energies $E_P/M_P>100$ keV/u. Furthermore, at such high velocities, β depends very weakly on the projectile velocity. This is an important assumption in the following discussion and needs further theoretical substantiation.[15] However, this assumption has been shown to be correct over a very broad range of proton energies (10 keV–24 MeV),[15,16,24,50] and thus seems to be a realistic approach. Below $E_P/M_P=100$ keV/u, the factors β_F and β_B are increased due to recoil-ion production related to the nuclear stopping. Thus, increased SE yields can be expected in this low-velocity region, in agreement with our experimental findings (Secs. III A and III B).

At higher velocities $\frac{1}{2}v_P^2=E_P/M_P>100$ keV/u, β describes the energy transport by recoiling electrons away from the upstream near-surface region or into the downstream near-surface region. The values of β are expected to fall in the interval $0.25<\beta<0.5$ for protons.[45] From symmetry arguments follows[44,45]

$$1-\beta_F=\beta_B:=\beta\ .\tag{7}$$

From Eq. (6) we obtain for fast proton impact

$$R=\gamma_F/\gamma_B=\beta_F/\beta_B=(1-\beta)/\beta\ .\tag{8}$$

Thus, we can easily obtain β by measuring the forward to backward SE yield ratio R for fast protons where $q_{\mathrm{eff},F}=q_{\mathrm{eff},B}=1$. In this case we obtain by comparison from Eqs. (2), (6), and (7)

$$\Lambda=\Lambda_F^*(H)/(1-\beta)=\Lambda_B^*(H)/\beta=\Lambda_T^*(H)\ .\tag{9}$$

From the proton data obtained with the present experimental setup[40] we obtain $R\approx1.2$. Then, according to Eqs. (7) and (8), we find that $\beta=\beta_B\approx0.45$ and $\beta_F\approx0.55$.

In case (iii) of Sec. III B we have shown that the $\Lambda_{F,B}^*$ are different for projectiles of different nuclear charge Z_P (H, He, and "heavy ions"). Thus $\Lambda_{T,F,B}^*$ introduced in Eq. (2) are no real "material parameters." As discussed above, the coefficients $\beta_{F,B}$ are only relevant for electron transport and can be expected to depend weakly on the ion-target combination at sufficiently high velocities. Thus, as it is in our interest to use a universal material parameter Λ, as it was determined from measurements with protons, i.e., we assume $\Lambda(Z_P)=$ const, we can easily extend our discussion within the transport theory to $Z_P>1$ by introducing Z_P dependent factors $C_F(Z_P)$ and $C_B(Z_P)$ in Eq. (6),

$$\begin{aligned}\gamma_F&=\Lambda(Z_T)(1-\beta)C_F(Z_P)S_e\ ,\\ \gamma_B&=\Lambda(Z_T)\beta C_B(Z_P)S_e\ .\end{aligned}\tag{10}$$

Note that Eq. (6) is valid for proton impact only, whereas Eq. (10) also holds for heavy-ion-induced SE yields. Then, as β does not depend on Z_P, we can obtain the factors $C_{F,B}(Z_P)$ empirically from the present measurements with heavy ions and the proton data of Ref. 40 by comparing heavy-ion-induced with proton-induced SE yield to energy-loss ratios,

$$\begin{aligned}C_F&=\Lambda_F^*(Z_P\geq1)/\Lambda_F^*(Z_P=1)\ ,\\ C_B&=\Lambda_B^*(Z_P\geq1)/\Lambda_B^*(Z_P=1)\ .\end{aligned}\tag{11}$$

The parameters C obtained in this way are listed in Table II for protons ($C=1$ by definition), He, and "heavy" projectiles (HI).

It is now clear that Λ defined by Eqs. (9) and (10) is a fundamental, "true" material parameter with $\Lambda=f(Z_T)$ and $\Lambda(v_P,Z_P)=$ const, i.e., Λ does not depend on the projectile velocity nor on the projectile nuclear charge, but on the target material. This material parameter Λ can be obtained by measurements with protons traversing foils with cleaned surfaces of different materials with sufficiently high projectile velocities ($v_P^2>100$ keV/u) such that one can assume charge equilibrium with $q_{\mathrm{eff},F}=q_{\mathrm{eff},B}=1$. Material parameters obtained in this way have recently been published by Clouvas *et al.*[24]

From Eqs. (6) and (9) it is clear that the measurement of proton-induced total SE yields $\gamma_T=\gamma_B+\gamma_F$ from thin

TABLE II. Energy-loss reduction factors $C_B=\Lambda_B^*(Z_P)/\Lambda_B^*(\mathrm{H})=S_{eB}^*/S_e$ and $C_F=\Lambda_F^*(Z_P)/\Lambda_F^*(\mathrm{H})=S_{eF}^*/S_e$ for the studied target materials (C, Al, Ti, Ni, and Cu); see text, Sec. IV C. Also, a mean value averaged over the values for the different target materials is included.

Target	Protons	Helium	Heavy ions
	$C_B=\Lambda_B^*(Z_P)/\Lambda_B^*(\mathrm{H})=S_{eB}^*/S_e$		
C	1	0.53	0.33
Al	1	0.58	0.28
Ti	1	0.65	0.44
Ni	1	0.54	0.38
Cu	1	0.71	0.42
Mean Value	1	0.60±0.08	0.32±0.07
	$C_F=\Lambda_F^*(Z_P)/\Lambda_F^*(\mathrm{H})=S_{eF}^*/S_e$		
C	1	0.68	0.50
Al	1	0.56	0.37
Ti	1	0.65	0.50
Ni	1	0.63	0.53
Cu	1	0.72	0.54
Mean value	1	0.65±0.06	0.49±0.07

foils is more "fundamental" and convenient (within the transport theory) than the measurement γ_B from thick samples. In the latter case uncertainties may arise because a detailed knowledge of the factor β is needed to calculate the material parameter Λ, whereas this is not needed in the former case due to the symmetry relation Eq. (7).

The important Eqs. (10) are based on the following assumptions.

(i) According to Schou, the contribution of "cascade electrons" from secondary ionization [step (b) mentioned in the Introduction] to the total yield is the dominant contribution to the SE yields both in forward and backward directions and thus the energy distribution of low-energy "true SE" is similar for all projectiles. Although there are no principal differences in the shapes of SE spectra for different projectiles at low velocities,[16] this remains to be shown for heavy ions at higher velocities, and in particular in the forward direction. The low-energy part of the SE spectrum can also be strongly influenced by collective excitations. Recent measurements show that plasmon decay can contribute to SE emission in an order of magnitude of some percent, or even more,[55,56] but cascade electrons seem to be dominant.

(ii) The parameter β is assumed to be independent of the type of projectile, i.e., the energy transport by electrons is "protonlike" and independent of the production. This is a simplification, because, e.g., the ejection of projectile electrons carried by incident heavier ions may transport energy away from the surface. Furthermore, in the case of heavy ions, the influence of the ion-induced wake has to be considered.[11–14] However, the assumption is supported by the experimental finding of similar β values for proton impact [$\beta\approx 0.45$ (Ref. 40)], heavy-ion impact [$\beta\approx 0.4$ (Ref. 35)], and by the calculations shown in Ref. 44.

The parameters $C(Z_P)$ include all projectile excitation, charge nonequilibrium, and screening effects. Their physical interpretation may be that they describe how effectively, compared to protons, the heavy-ion energy loss can be transferred into kinetic energy of electrons.[15]

Another possible point of view is that C values describe a ratio between the *tabulated bulk energy loss* values and a *"nonequilibrium near-surface energy loss"* both at the upstream and the downstream surface of the foils under the assumption of a proportionality of γ and S_e (compare Sec. IV A). A similar view has recently been successfully applied to interpret target-thickness-dependent SE yields.[32] In this contect, the term "near-surface" means within a depth comparable to the characteristic electron-transport lengths λ_{SE} and λ_δ and the charge equilibration mean free path, i.e., some ten to some hundred angstroms. It is important to note that the energy loss of ions depends on projectile electron-loss and target-electron capture processes (charge-changing energy loss).[57–59] In particular, the energy loss is correlated to the nonequilibrium process of the evolution of the ionic charge state near the entrance surface[32,58,59] and to the dynamic self-screening of the projectile by bound projectile electrons.[32,60]

Deviations of up to a factor of 2 occur between the near-surface energy loss and the tabulated bulk energy loss (under the assumption of a proportionality between SE yield and electronic stopping). This is true both near the entrance and the exit surface. The parameters C describe in a very general way a variety of possible physical mechanisms that can possibly cause a projectile dependence of an effective energy loss near the entrance or exit surface; possibly, e.g., charge exchange, screening effects, projectile excitation or ionization, or even molecular-orbital excitation effects may contribute to the Z_P dependence.

An evolution of the "effective" projectile charge occurs at the entrance surface of the foil within some few atomic layers until the bulk effective charge value is reached, but also at the exit surface where a sudden change of the projectile screening or a deexcitation of the projectile having been excited inside the solid can take place.[59] Also, modifications of the surface potential barrier[26,35] and a strong positive charging up near the ion track[30,35] have been discussed in this context.

Furthermore, the excitation or ionization probabilities of projectile electrons increase with the number of electrons, i.e., Z_P.[15,61] The deexcitation of the projectile when exiting the foil can contribute to enhanced SE emission in the forward direction and indeed, from Table II we see that $C_F > C_B$. Here, one could argue that the charge state of the incoming ions was $q_i=1$ in the present experiment, and that bare projectiles should lead to a higher effective charge near the surface and thus a higher energy loss leading to enhanced SE yields. This is true at higher ion velocities,[32] but such effects are small ($<10\%$) at the lower velocities used in the present experiment.[38,39] Also, the projectiles are charge equilibrated within path lengths shorter than δ-electron ranges.[62]

Thus, the effective ionic charge inside the bulk of the solid generally differs from both the mean charge of the

ions after exiting the foil and the charge of the incoming ions. The most important charge exchange and deexcitation processes must happen very near the surface. In this context, it would be interesting to study heavy-ion-induced SEE from thin foils at higher projectile velocities ($>$MeV/u) as a function of the ionic charge state and the target thickness from sputter-cleaned, controlled surfaces.

Promising attempts have recently been made by Koschar and co-workers[32] to connect nonequilibrium stopping powers with SE emission. Their model can also be applied in the present case. From Ref. 32 we obtain

$$\gamma_B \sim S_{eB}^* ,$$
$$\gamma_F \sim S_{eF}^* , \tag{12}$$

and the quantities $C_F S_e \sim S_{eF}^*$ and $C_B S_{eB} \sim S_{eB}^*$ can be interpreted as nonequilibrium energy losses near the surface similar to Allison's partial stopping-power concept.[57] The target thickness dependence and probably the velocity dependence of SE yields can thus be used to study effective stopping powers of ions in condensed matter and to compare these with those in the gas phase. This may help to clarify the importance of solid-state or phase effects.[63]

With Eq. (10) we can describe the Z_P dependence of $R(Z_P)=\gamma_F/\gamma_B$ with $\beta=0.45$,

$$R=\gamma_F/\gamma_B=1.2C_F/C_B \tag{13}$$

and with the mean C values from Table II we find $R(\mathrm{H})=1.2$, $R(\mathrm{He})=1.3$, and $R(\mathrm{HI})=1.9$, in agreement with the experimental findings (Fig. 11). Thus, an essential proportion of the Z_P dependence of R is caused by differences in the effectivity of SE creation near the surfaces, which in turn is determined by the respective effective projectile energy losses. The enhancement of $\gamma_F=1.2\gamma_B$ for protons and a corresponding fraction of the enhancement for heavier ions is caused by additional SE creation in the forward direction by fast δ electrons.

With the R values from Eq. (13) together with $\lambda_{SE}/\lambda_\delta$ for $E_P/M_P \approx 0.1$ MeV/u taken from Eq. (5), we find on the other hand $B(\mathrm{He})\approx 0.45$ and $B(\mathrm{HI})\approx 0.42$ [compare with Eq. (3), Sec. IV A]. Surprisingly, these values are close to the equipartition $B=0.5$ chosen by Sternglass.[43]

D. Proportionality between secondary-electron yield and stopping power

Finally, if we express Λ in units of Å/eV rather than in units of $(\mu g/cm^2)/eV$, i.e., if we take into account the different densities of the targets and relate γ to the "energy loss per unit path length" dE/dx and not to the "stopping cross section" $(dE/dx)N$, we find interestingly very similar Λ values for all studied target materials. Our mean value is $\Lambda=0.32$ Å/eV with $Z_T=6,22,28,29$ (Table I). This is in good agreement with mean values of Λ given by Clouvas *et al.*[24] ($\Lambda=0.31$ Å/eV; $Z_T=28,29,46,47,61,63,79,83$) and Schou[45] ($\Lambda=0.29$ Å/eV; $Z_T=4,12,13$).

In spite of the systematic deviations concerning the Z_P and Z_T dependences discussed in this paper, the important assumption of an overall proportionality between SE yields and the electronic energy loss of the projectiles [Eq. (1)] is demonstrated impressively in Fig. 12, which shows the total secondary-electron yield γ_T from carbon foils as a function of the electronic energy loss taken from Ref. 65. A similar plot was first given by Frischkorn and Groeneveld,[23] and is enriched here with further data. We have included the data given in Refs. 23, 24, and 40, data from the present work, and as yet unpublished data obtained by our group. We can state a rough proportionality $\gamma_T \sim dE/dx$ within a factor of 2 in a wide range of projectile velocities 15 keV/u $\le E_P/M_P \le$ 16 MeV/u and projectile nuclear charges $1 \le Z_P \le 92$ over four decades of secondary-electron yields γ and electronic energy losses dE/dx.

Again, we find a mean value of $\Lambda_T^*=0.31$ Å/eV. The deviations within a factor of 2 from this mean material parameter can be attributed to the Z_P and Z_T dependence of Λ^* (see Secs. IV B and IV C), whereas the velocity dependence $\Lambda^*(v_P)=$ const is confirmed; see above (Sec. IV A). It would be interesting to complete the findings of Fig. 12, in particular, by extending the measurements towards both lower and higher dE/dx values. This can be done by measuring SE yields at higher projectile velocities v_P (MeV/u range) with both light and heavy ions.

The findings from Fig. 12 together with the results from Table II allow us to give a simple relationship for an estimate of secondary-electron yields γ_B and γ_F from metallic solids and solid foils, not only for protons (H),

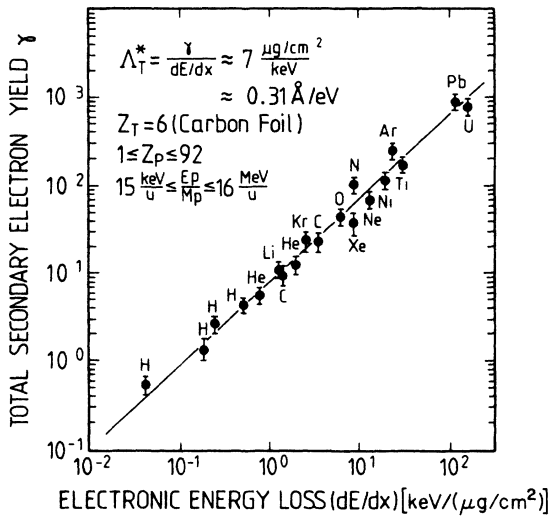

FIG. 12. The total secondary-electron yield γ_T from carbon foils as a function of the electronic energy loss dE/dx of the projectiles taken from Ref. 65. Data from Refs. 23, 24, and 40, as well as data from the present work and as yet unpublished data have been included. The projectiles (15 keV/u $\le E_P/M_P \le$ 16 MeV/u, $1 \le Z_P \le 92$) are indicated in the figure. It is important to note that the data were taken with incident charge states q_i close to the mean charge state q_f of the emerging ions.

but also for He and heavy-ion (HI) impact,

$$\gamma_B = 0.14 C_B dE/dx$$
$$\text{with } C_B(\text{H})=1,\quad C_B(\text{He})=0.6,\quad C_B(\text{HI})=0.3\ , \tag{14}$$
$$\gamma_F = 0.17 C_F dE/dx$$
$$\text{with } C_F(\text{H})=1,\quad C_F(\text{He})=0.65,\quad C_F(\text{HI})=0.5\ ,$$

with dE/dx measured in units of eV/Å. Equation (14) can be applied in the specific energy range above, say, 50 keV/u and can be expected to give reasonable results up to the MeV/u range. The accuracy is ±20% for H, ≈±40% for He, and should be accurate within a factor of 2 for heavy ions with $Z_P \leq 36$. For heavier ions, and at much lower or much higher velocities as well as for contaminated surfaces, major deviations are likely to occur.

V. CONCLUSION AND OUTLOOK

We have studied the v_P, Z_P, and Z_T dependences of heavy-ion-induced secondary-electron yields γ_B and γ_F from the sputter-cleaned entrance and exit surfaces of thin foils in ultrahigh vacuum. The forward to backward SE yield ratio $R=\gamma_F/\gamma_B$, and the SE yield to energy-loss ratio $\Lambda^*=\gamma/S_e$ have been deduced from the measurements. In the studied parameter range, Λ^* has been found to be independent of the projectile velocity v_P for sufficiently high projectile velocities, $E_P/M_P=v_{P^2}>50$ keV/u, i.e., $\Lambda^*(v_P)=$ const, even for heavy ions (HI). However, Λ^* depends on the projectile nuclear charge Z_P [$\Lambda^*(\text{HI})<\Lambda^*(\text{He})<\Lambda^*(\text{H})$]. Also, a pronounced increase of R with Z_P has been observed.

The velocity and projectile dependence of both $\Lambda^*_{F,B}$ and R can qualitatively be understood within an extended semiempirical Sternglass-type SE emission model by Koschar *et al.*[32,43] In the context of Schou's transport theory,[44,45] we describe these dependencies as caused in part by differences in the energy transport of internally produced SE, but also by a reduced energy loss S_e^* of the projectiles compared to tabulated bulk energy-loss values S_e. The reduced stopping power S_e^* is (i) an effective, (ii) a charge nonequilibrium, and (iii) a near-surface quantity. The Z_P-dependent reduction factors $C=S_e^*(Z_P)/S_e$ as well as material parameters Λ and a simple relationship for an estimate of SE yields γ_B and γ_F are given.

We finally present evidence for a rough proportionality—within a factor of 2—between SE yields and the electronic energy loss of the projectiles in a wide range of projectile velocities and projectile nuclear charges Z_P over four decades of γ and dE/dx values.

The measurement of SE yields from thin foils, in particular, as a function of the incident ionic charge state q_i and the target thickness d, can provide valuable information on nonequilibrium stopping powers and electron transport in solids.[32,48] The application of both transport[44] and semiempirical[32,43] theory to heavy-ion-induced SE emission leads to promising results. Further studies of SE yields γ_F and γ_B from thin foils are necessary, in particular, at higher projectile velocities with heavier ions possibly under frozen charge-state conditions, which become accessible with the recently developed heavy-ion accelerators. Also, a simultaneous measurement of SE yields and the energy loss for all kinds of projectiles in a wide velocity range appears to be desirable.

Open questions, as e.g., the contribution of recoil ions, "true" cascade electrons, or collective excitations to the SE yields and also the role of projectile ionization and excitation (see Secs. IV A and IV B) can probably be answered by studying the d, q, v_P, Z_P, and Z_T dependence of secondary-electron energy and angular distributions from clean thin foils with light and heavy ions,[29] performed under ultrahigh-vacuum conditions. SE energy and angular distributions yield more detailed information about SE emission, because they exhibit several important structures[29] as, e.g., the "true cascade SE" peak at low electron energies $E_e<10$ eV, the binary encounter electron peak at $v_e=2v_P\cos\theta$ (v_e, electron velocity; θ, observation angle), characteristic target and possibly projectile Auger electrons,[8,15] convoy electrons at $v_e=v_P$ ($\theta=0°$), loss electrons from heavy or molecular ions at $v_e=-v_P$ around $\theta=180°$ (backward direction), and low-energy peaks ($E_e<25$ eV) resulting from the one-electron decay of plasmons.[16,56] Another collective effect, the emission of shock electrons perpendicular to the ion-induced wake in the electron plasma of the solid, can be observed in angular distributions.[11–13] In particular, it will be interesting to compare such SE spectra induced by isotachic electrons, protons, and heavy ions.[45] Also studies of the temperature dependence of both SE yields and SE energy and angular distributions, not only from metals,[29] but even from superconductors,[30] can yield further information about SE emission.

ACKNOWLEDGMENTS

It is a pleasure for us to thank J. Schou (Risø, Denmark) for fuitful discussions and helpful suggestions concerning the application of his transport theory to heavy-ion-induced secondary-electron emission. One of us (A.C.) is grateful to his German colleagues for their constant hospitality and to the Johann-Wolfgang-Goethe-Universität (Frankfurt am Main, Federal Republic of Germany) for financial support. One of us (E.V.) is grateful to the Institut für Kernphysik in Frankfurt am Main for the great hospitality he enjoyed during his stay, as well as for financial support from the Julie Damms Foundation. This work has been funded by the Bundesminister für Forschung und Technologie, Bonn, Federal Republic of Germany, under Contract No. 06 OF 110/II Ti 476.

*Permanent address: Aristotelian University of Thessaloniki, Faculty of Technology, Department of Eelctrical Engineering, Section of Electrical Energy, GR-540 06 Thessaloniki, Greece.

†Permanent address: Physics Laboratory, H. C. Ørsted Institute, Universitetsparken 5, DK-2100 Copenhagen, Denmark.

‡Permanent address: Instituto Balseiro y Centro Atómico de Bariloche, 8400 S.C. de Bariloche, Argentina.

[1]P. Sigmund and S. Tougaard, in *Inelastic Particle-Surface Collisions,* Vol. 17 of *Springer Series in Chemical Physics,* edited by E. Taglauer and W. Heiland (Springer-Verlag, Berlin, 1981), p. 2.

[2]M. Inokuti, in *Applied Atomic Collision Physics, Vol. 4: Condensed Matter,* edited by H. S. W. Massey *et al.* (Academic, New York, 1983), p. 179.

[3]W. Brandt and R. H. Ritchie, U.S. Atomic Energy Commission, Report No. CONF-721 001 (1974), p. 20.

[4]W. O. Hofer, J. Vac. Sci. Technol. A **5**, 2213 (1987).

[5]K. Ertl and W. Behrisch, in *Physics of Plasma-Wall Interactions in Controlled Fusion,* edited by D. E. Port and R. Behrisch, (Plenum, New York, 1986), p. 515.

[6]K. O. Groeneveld, Nucl. Tracks Radiat. Meas. **15**, 51 (1988).

[7]K. Wien, O. Becker, W. Guthier, S. Della-Negra, Y. LeBeyec, B. Monart, K. Standing, G. Maynard, and C. Deutsch, Int. J. Mass Spectrom. Ion Phys. **78**, 273 (1987).

[8]M. Burkhard, H. Rothard, J. Kemmler, K. Kroneberger, and K. O. Groeneveld, J. Phys. D **21**, 472 (1988).

[9]P. Lorenzen, H. Rothard, K. Kroneberger, J. Kemmler, M. Burkhard, and K. O. Groeneveld, Nucl. Instrum. Methods A **282**, 213 (1989).

[10]*Forward Electron Emission in Ion Collisions,* edited by K. O. Groeneveld, W. Meckbach, and I. A. Sellin (Springer-Verlag, Heidelberg, 1984).

[11]M. Burkhard, H. Rothard, C. Biedermann, J. Kemmler, K. Kroneberger, P. Koschar, O. Heil, and K. O. Groeneveld, Phys. Rev. Lett. **58**, 1773 (1987).

[12]H. Rothard, M. Burkhard, J. Kemmler, C. Biedermann, K. Kroneberger, P. Koschar, O. Heil, and K. O. Groeneveld, J. Phys. (Paris) Colloq. **48**, C9-211 (1987).

[13]H. Rothard, K. Kroneberger, M. Burkhard, C. Biedermann, J. Kemmler, O. Heil, and K. O. Groeneveld, J. Phys. (Paris) Colloq. **50**, C2-105 (1989).

[14]P. M. Echenique, R. H. Ritchie, and W. Brandt, Phys. Rev. B **20**, 2567 (1979).

[15]D. Hasselkamp, Habilitationsschrift, Justus-Liebig-Universität, Giessen, West Germany, 1985).

[16]D. Hasselkamp, Comments At. Mol. Phys. **21**, 241 (1988).

[17]M. P. Villard, J. Phys. Theor. Appl. **8**, 5 (1899).

[18]J. J. Thomson, Proc. Cambridge Philos. Soc. **13**, 49 (1904).

[19]E. Rutherford, Philos. Mag. **10**, 193 (1905).

[20]C. Füchtbauer, Phys. Z. **7**, 153 (1906).

[21]G. Schneider, Ann. Phys. **5**, 357 (1931).

[22]J. Schader, B. Kolb, K. D. Sevier, and K. O. Groeneveld, Nucl. Instrum. Methods **151**, 563 (1978).

[23]H. J. Frischkorn and K. O. Groeneveld, Phys. Scr. **T6**, 89 (1983).

[24]A. Clouvas, H. Rothard, M. Burkhard, K. Kroneberger, R. Kirsch, P. Misealidis, A. Katsanos, C. Biedermann, J. Kemmler, and K. O. Groeneveld, Phys. Rev. B **39**, 6316 (1989).

[25]H. P. Garnir, P. D. Dumont, and Y. Baudinet-Robinet, Nucl. Instrum. Methods **202**, 187 (1982).

[26]H. J. Frischkorn, K. O. Groeneveld, P. Koschar, R. Latz, and J. Schader, Phys. Rev. Lett. **49**, 1671 (1982); H. J. Frischkorn, P. Koschar, J. Kemmler, R. Latz, J. Schader, and K. O. Groeneveld, Nucl. Instrum. Methods **B2**, 35 (1984).

[27]H. G. Clerc, H. J. Gerhardt, L. Richter, and K. H. Schmidt, Nucl. Instrum. Methods **113**, 325 (1973).

[28]T. J. Gay and H. G. Berry, Phys. Rev. A **19**, 952 (1979); J. Phys. (Paris) Colloq. **40**, C1-298 (1979).

[29]H. Rothard, K. Kroneberger, P. Lorenzen, E. Veje, N. Keller, R. Maier, M. Schosnig, C. Biedermann, A. Albert, J. Kemmler, O. Heil, and K. O. Groeneveld, Institut für Kernphysik der Johann-Wolfgang-Goethe-Universität Annual Report No. **IKF-48**, 1988 (unpublished), p. 42; H. Rothard, K. Kroneberger, M. Schosnig, P. Lorenzen, E. Veje, N. Keller, R. Maier, J. Kemmler, C. Biedermann, A. Albert, O. Heil, and K. O. Groeneveld, Nucl. Instrum. Methods B (to be published).

[30]H. Rothard, P. Lorenzen, N. Keller, O. Heil, D. Hofmann, J. Kemmler, K. Kroneberger, S. Lencinas, and K. O. Groeneveld, Phys. Rev. B **38**, 9224 (1988).

[31]K. Kroneberger, A. Clouvas, G. Schlüssler, P. Koschar, J. Kemmler, H. Rothard, C. Biedermann, O. Heil, M. Burkhard, and K. O. Groeneveld, Nucl. Instrum. Methods **B29**, 621 (1988).

[32]P. Koschar, K. Kroneberger, A. Clouvas, R. Schramm, M. Burkhard, O. Heil, J. Kemmler, H. Rothard, H. D. Betz, and K. O. Groeneveld, Phys. Rev. A **40**, 3632 (1989).

[33]K. E. Pferdekämper and H. G. Clerc, Z. Phys. **A275**, 223 (1975); **280**, 155 (1977).

[34]W. Meckbach, G. Braunstein, and N. Arista, J. Phys. B **8**, L344 (1975).

[35]A. Koyama, T. Shikata, H. Sakairi, and E. Yagi, Jpn. J. Appl. Phys. **21**, 1216 (1982).

[36]C. R. Shi, H. S. Toh, D. Lo, R. P. Livi, M. H. Mendenhall, D. Z. Zhang, and T. A. Tombrello, Nucl. Instrum. Methods **B9**, 263 (1985).

[37]J. C. Dehaes, J. Carmeliet, and A. Dubus, Nucl. Instrum. Methods **B13**, 627 (1986).

[38]C. C. Dednam, S. Froneman, D. W. Mingay, and J. Van Waart, Nucl. Instrum. Methods **B24/25**, 366 (1987).

[39]E. F. da Silveira and J. M. F. Jeronymo, Nucl. Instrum. Methods **B24/25**, 534 (1987).

[40]H. Rothard, K. Kroneberger, M. Burkhard, J. Kemmler, P. Koschar, O. Heil, C. Biedermann, S. Lencinas, N. Keller, P. Lorenzen, D. Hofmann, A. Clouvas, K. O. Groeneveld, and E. Veje, Radiat. Eff. Defects Solids **109**, 287 (1989).

[41]K. Kroneberger, H. Rothard, M. Burkhard, J. Kemmler, P. Koschar, O. Heil, C. Biedermann, S. Lencinas, N. Keller, P. Lorenzen, D. Hofmann, A. Clouvas, E. Veje, and K. O. Groeneveld, J. Phys. (Paris) Colloq. **50**, C2-99 (1989).

[42]H. Rothard, K. Kroneberger, E. Veje, J. Kemmler, P. Koschar, O. Heil, S. Lencinas, N. Keller, P. Lorenzen, D. Hofmann, A. Clouvas, and K. O. Groeneveld, Phys. Rev. B (to be published).

[43]E. J. Sternglass, Phys. Rev. **108**, 1 (1957).

[44]J. Schou, Phys. Rev. B **22**, 2141 (1980).

[45]J. Schou, Scanning Electron Microsc. **2**, 607 (1988).

[46]J. Devooght, A. Dubus, and J. C. Dehaes, Phys. Rev. B **36**, 5093 (1987).

[47]M. Rösler and W. Brauer, Phys. Status Solidi B **148**, 213 (1988).

[48]J. Kemmler, thesis, Johann-Wolfgang-Goethe-Universität, Frankfurt am Main, West Germany, 1988.

[49]G. Holmén, B. Svensson, J. Schou, and P. Sigmund, Phys. Rev. B **20**, 2247 (1979).

[50]J. E. Borovsky, D. J. McComas, and B. L. Barraclough, Nucl. Instrum. Methods **B30**, 191 (1988).

[51]H. Rothard, M. Burkhard, C. Biedermann, J. Kemmler, P. Koschar, K. Kroneberger, O. Heil, D. Hofmann, and K. O. Groeneveld J. Phys. C **21**, 5033 (1988).

[52]J. F. Ziegler, J. P. Biersack, and U. Littmark, *The Stopping and Range of Ions in Matter* (Pergamon, New York, 1985).

[53]N. Bohr, K. Dan. Vidensk. Selsk. Mat.-Fys. Medd. **18**, No. 8 (1948).

[54]S. Hippler, D. Hasselkamp, and A. Scharmann, Nucl. Instrum. Methods **B34**, 518 (1988).
[55]M. Burkhard, H. Rothard, and K. O. Groeneveld, Phys. Status Solidi B **147**, 589 (1988).
[56]S. Hippler, thesis, Justus-Liebig-Universität, Giessen, West Germany, 1988.
[57]J. Cuevas, M. Garcia-Munoz, P. Torres, and S. K. Allison, Phys. Rev. **135**, A335 (1964).
[58]L. B. Bridwell, N. E. B. Cowern, P. M. Read, and C. J. Sofield, Nucl. Instrum. Methods **B13**, 123 (1986) and references therein.
[59]H.-D. Betz, Rev. Mod. Phys. **44**, 465 (1972).
[60]W. Brandt in *Atomic Collisions in Solids,* edited by S. Datz *et al.* (Plenum, New York, 1975), Vol. 1, p. 261.
[61]F. Thum and W. O. Hofer, Nucl. Instrum. Methods **B2**, 531 (1984).
[62]C. Biederman, J. Kemmler, H. Rothard, M. Burkhard, O. Heil, P. Koschar, K. Kroneberger, and K. O. Groeneveld, Phys. Scr. **37**, 27 (1988).
[63]J. R. Sabin and J. Oddershede, Nucl. Instrum. Methods **B36**, 249 (1989).
[64]B. Svensson and G. Holmén, J. Appl. Phys. **52**, 6928 (1981).
[65]L. C. Northcliffe and R. F. Schilling, Nucl. Data Tables **A7**, 253 (1970).